ARGONNE NATIONAL LABORATORY
9700 South Cass Avenue
Argonne, Illinois 60439

Development of a fast, robust numerical tool for the design, optimization, and control of IC engines

Shashi M. Aithal[1] **and Stefan M. Wild**[2]

Mathematics and Computer Science Division

Preprint ANL/MCS-P4051-0313

March 2013, *revised August 2013*

[to appear in Proceedings of the SAE 11th International Conference on Engines & Vehicles (ICE2013), Capri, Italy, September 2013]

`http://www.mcs.anl.gov/publications/`

[2]Mathematics and Computer Science Division, Argonne National Laboratory, Argonne, IL 60439, USA

[1]Computing, Environmental, and Life Sciences Directorate, Argonne National Laboratory, Argonne, IL 60439, USA

2013-24-0141

Development of a fast, robust numerical tool for the design, optimization, and control of IC engines

S. M. Aithal
Computing, Environmental, and Life Sciences Directorate

S. M. Wild
Mathematics and Computer Science Division

Argonne National Laboratory

Argonne, IL 60439

ABSTRACT

This paper discusses the development of an integrated tool for the design, optimization, and real-time control of engines from a performance and emissions standpoint. Our objectives are threefold: (1) develop a tool that computes the engine performance and emissions on the order of a typical engine cycle (25-50 milliseconds); (2) enable the use of the tool for a wide variety of engine geometries, operating conditions, and fuels with minimal user changes; and (3) couple the engine module to an efficient optimization module to enable real-time control and optimization.

The design tool consists of two coupled modules: an engine module and an optimization module. The engine module consists of three components: a two-zone quasi-dimensional engine model to compute the temporal variation of temperature and pressure during the compression and power stroke, a thermal model to compute the cyclic variation of the engine wall temperature, and a reaction-rate-controlled emission model to compute engine-out NO and CO. The optimization solver is an extension of the model-based, derivative-free POUNDER and is designed to limit the number of engine model evaluations. The outputs of the engine model, thermal model, and emissions model can be used for optimizations under various design constraints.

By more thoroughly using the output from the simulations, our optimization scheme reduces the number of simulation evaluations by two orders of magnitude compared with parameter sweeps and one order of magnitude compared with the standard black-box optimizer in MATLAB. These results highlight the proposed tool's potential for use in design, optimization, and real-time control of engines.

INTRODUCTION

Modern automotive engines (both SI and CI) are complex systems that pose several multiobjective, multiconstraint problems from an engine control and optimization standpoint. These are largely due to the ever-increasing demand for higher power output, increased fuel economy, and reduced emissions. Real-time control of IC engines poses even greater challenges in terms of computational cost, robustness of the control algorithms, and fidelity of the underlying physical models. Given the large parameter space (engine geometry, engine RPM, air-fuel-ratio, spark/fuel injection timing, etc.) over which an engine has to be optimized for performance and emissions, formulation of a generalized mathematical optimization problem can be difficult. Typically, design engineers focus on examining localized regions of the overall operating parameter space in order to evaluate the relative effect of changing one particular parameter with respect to another. For instance, one could pose questions such as *What is the minimum percent reduction in engine torque needed in order to obtain a 2 percent reduction in fuel consumption?* or *What is the percent increase in overall engine-out NO/CO for a 5 percent increase in overall average torque over a typical driving cycle?* Design, optimization, and control of conventional engines can be carried out by using available engine data. For newer engine concepts and/or operating regimes and for engines powered by alternative fuels or fuel blends, one can complement limited engine data through the use of reliable physics-based engine models for making design and/or optimization decisions. Development of reliable, physics-based engine modeling tools can thus play an integral role in the design and optimization studies of engines.

Transient multidimensional numerical simulation of the entire engine cycle that models the effects of complex

combustion chemistry and turbulence is extremely challenging. Such simulations can take several hours to days, depending on factors such as complexity of the flow or chemistry model and size of the computational domain. Hence, the required computational effort precludes using multi-dimensional simulations in the early stages of design, development, and engine optimization in terms of performance and emissions. On the other hand, computationally fast, robust, physics-based, quasi-dimensional modeling tools require minimal computational resources, and the computational time for solutions is usually on the order of seconds. Development of such quasi-dimensional modeling tools can greatly aid the design, analysis, and optimization of IC engines. Several quasi-dimensional models have been developed since the early 1980s to study both gasoline and diesel engines (see, for example, [1-8]) with varying degrees of fidelity. With few exceptions (for instance, [3] and [7]), however, these studies do not discuss the wall-clock time required for the computation of an engine cycle (a single compression and expansion stroke). The level of fidelity in the quasi-dimensional model and the wall-clock time required for the computation of an engine cycle are important considerations, especially for real-time optimization and control, which require the computational time to be on the order of an engine cycle (typically, 25-50 milliseconds). In this paper we discuss a methodology to greatly increase the computational speed of engine optimization problems by using a fast, robust engine module designed for use with an efficient optimization scheme.

Several investigators have published results for engine optimization based on various optimization techniques [9-21]. Most of these studies discuss optimization of engine performance alone. Relatively fewer studies report on engine optimization from both a performance and an emissions standpoint [19-21]. These latter optimization studies have focused primarily on black-box global optimization algorithms, such as genetic algorithms, particle swarm optimization, simulated annealing, and the DIRECT method [22-24]. Although their internal optimization parameters must often be tuned to the particular problem, these methods tend to be robust to computational noise and discontinuities, provided the number of parameters is small (typically 1-3) or a large number of simulation evaluations (often in the millions) are possible.

In this paper we consider local optimization methods, which begin from a user-provided initial design vector and search for a local minimum/maximum. Because these methods do not need to asymptotically obtain a global solution, they require fewer simulation evaluations than do their global counterparts. We restrict our focus to so-called derivative-free methods [25], which operate even when the objective and/or constraint function derivatives with respect to the design parameters are unavailable. Under idealized circumstances, the dependence of the underlying differential algebraic equations (DAEs) on the design parameters is algebraically available to first order; and derivative-based or even linear programming methods could be employed (see, e.g., [26]). Alternatively, when explicit derivatives are unavailable, algorithmic (sometimes called "automatic") differentiation (AD) is often a viable option [27]. We focus on the derivative-free case in recognition of many of the practical obstacles that remain, such as truncation of crank angle degrees and look-up tables based on experimental data. Within the class of derivative-free local optimization methods, we focus on model-based methods, which have been shown to perform well when relatively few simulation evaluations are available [28]. These methods seek to fully exploit the information obtained from each simulation evaluation by building local surrogate models based on the simulation output. Another benefit of these methods is that they can exploit additional knowledge of structure (temporal variation of temperature/pressure, derived quantities such as engine torque, emissions, etc.) in the problem, rather than aggregating the simulation output into a single "black-box" scalar objective. Such information is often present in many real-world problems and can be used to further reduce the number of simulation evaluations required in order to solve the optimization problem and/or to obtain more accurate solutions. Our method employs quadratic interpolation models [29]. Examples of this approach exploiting structure include parameter fitting (nonlinear least squares) problems [30] and simulation-based, nonlinear constraints [31]. We illustrate its application here on a bilevel problem of determining the equivalence ratio at which engine-out NO is maximum under maximum brake torque (MBT) conditions.

The main focus of this work was to develop an integrated design tool with the following features: (1) a physics-based engine module where different components (or models) can be coupled or uncoupled easily, (2) flexibility and ease of use for exploring a large parameter space, (3) capability of computing performance and emission characteristics on the order of an engine cycle (25-50 milliseconds), and (4) use of inputs from the engine module to conduct optimization. Figure 1 shows a block diagram of the approach used in this work.

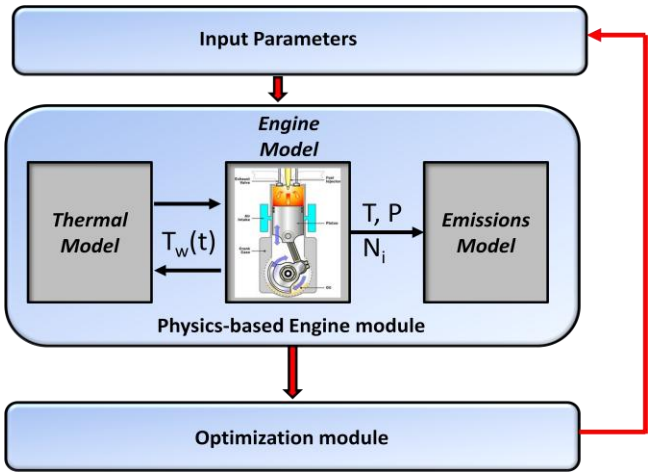

Figure 1: Block diagram showing the modules and models in the design/optimization tool.

The design/optimization tool presented here consists of two main modules: a physics-based engine module and an optimization module. The physics-based module has three main submodels: a two-zone quasi-dimensional engine model, a thermal model, and an emissions model for obtaining performance and emission quantities for the engine. The outputs of the engine module (namely, torque/BMEP/work and engine-out NO and/or CO) serve as inputs to the optimization module. The optimization module determines the next set of input parameters based on the objective function(s) and constraints. Unlike many studies that focus only on optimization of engine performance, this work includes an emissions model to compute engine-out emissions (NO and CO). The emissions model can easily be extended to include reduced-order soot/HC emissions as well. The thermal model is used to compute cylinder wall temperature, which can be coupled or uncoupled from the main engine model with relative ease. This module was included to enable evaluation of the impact of the coolant system on the overall fuel-economy of the engine.

Flexibility and ease of use are important considerations in the successful application of quasi-dimensional models for control and optimization studies. As shown in Figure 1, our design/optimization tool enables the user to enter geometrical and operating conditions (such as fuel/additive type, engine dimensions, air-fuel ratio, and injection/ignition timing, fuel-dependent combustion parameters) for a particular engine, which can be modified by the optimization module. Both these factors—computational speed and flexibility/ease of use—have been given prime importance in the development of the tool presented in this paper. Computational speeds of 8 milliseconds per engine cycle were obtained by using robust physics models and solution techniques for each of the components (engine, thermal, and emissions) of the engine module.

The engine model is a two-zone quasi-dimensional model wherein the energy equation is solved in order to compute the temporal variation of average engine cylinder pressure. The temporal variation of engine pressure can be used to compute the temporal variation of the burned and unburned gas temperatures in the cylinder. Effects of temperature and mixture composition on the thermophysical properties of the working fluid were included in the solution of the energy equation. Temporal variations of the thermophysical properties of all the species in the gas mixture were obtained by using thermodynamic coefficients from the CHEMKIN database. Most papers discussing quasi-dimensional engine models do not explicitly state the methodology used to compute γ (the ratio of specific heats). Many quasi-dimensional models use fixed values of γ during the compression and expansion strokes. Typically, γ is held constant at a value of 1.35 during the compression stroke and a value of 1.25 during the expansion stroke. This procedure leads to inaccurate values of cylinder pressure and temperature and hence the predicted emissions. Furthermore, the inaccuracies are more pronounced in engines using exhaust gas recirculation (EGR), as discussed in [32]. Knowledge of the temporal variation of cylinder pressure can be used to compute engine performance (quantities such as torque and BMEP). The thermal model is used to compute the temporal variation of the cylinder wall temperature. The thermal model solves the 1-D heat conduction equation by using the coolant temperature and engine gas temperature as the boundary conditions. The emissions model uses the temporal variation of temperature, pressure, burned gas volume, and burned gas composition to compute the temporal variation of NO and CO. NO and CO can be calculated by using the reaction-rate-controlled models or reduced finite-rate chemistry models. Engine geometry and operation conditions (such as cylinder pressure, inlet air temperature, EGR temperature, ignition timing/SOI, fuel and air mass), fuel type and combustion parameters (such as the Wiebe constants) are user-defined input parameters and supplied to the engine module. The optimization module can alter design parameters in the list of input parameters in order to maximize/minimize the objective function(s) and satisfy the design/system constraints.

MODEL DESCRIPTIONS

This section describes the two-zone quasi-dimensional engine model, the thermal model, the emissions model, and the optimization model used in this work.

Two-Zone Quasi-Dimensional Engine Model

A numerical model used to compute the temporal variation of temperature and pressure in a single-cylinder diesel engine was described in detail in [32]. As in that reference, the temporal variation of the engine pressure and temperature during the compression and power stroke was obtained by numerical solution of the energy equation. Effects of temperature and mixture composition on the thermophysical properties of the working fluid were included in the solution of the energy equation. Temporal variations of the thermophysical properties of all the species in the gas mixture were obtained by using thermodynamic coefficients from the CHEMKIN database (methane was used as a surrogate for natural gas for results shown in this paper). Following the procedure in [32], fuel combustion chemistry was modeled by a single-step global reaction. The combustion process of the premixed fuel-air mixture after the spark was modeled by using the well-known Wiebe function. The Wiebe function can be used to compute the mass of fuel burned at each crank angle and also the burned and unburned gas temperature. The equations describing the quasi-dimensional engine model and emissions model (presented next) are also described in a companion paper (2013-24-0134) and are repeated for the sake of completion and convenience of the reader.

The energy equation describing the variation of pressure with crank angle is as follows.

$$\frac{dP(\theta)}{d\theta} = \frac{\gamma - 1}{V(\theta)}\left(Q_{in} - Q_{loss}\right) - \gamma \frac{P(\theta)}{V(\theta)}\frac{dV}{d\theta} \quad (1)$$

The amount of heat produced (Q_{in}) due to the fuel burned ($m_{fb}(\theta)$) from θ to θ+dθ is given by

$$Q_{in}(\theta) = \left(H_P(T) - H_R(T)\right) \cong m_{fb}(\theta) LHV \tag{2}$$

while the heat lost from the engine during the interval is given by

$$Q_{loss}(\theta) = \frac{h_{cg} A}{\omega}\left(T(\theta) - T_w(t)\right) \tag{3}$$

The heat loss from the engine shown in Eq. (3) depends on the heat-transfer coefficient of the hot gases and the engine wall temperature. $T_w(t)$ (wall temperature) in Eq. (3) is a function of time. The transient engine wall temperature is obtained by the solution of a 1-D heat conduction equation described later.

The instantaneous values of volume, area, and displacement given by the slider-crank model [32] are as follows.

$$V(\theta) = V_c + \frac{\pi D^2}{4} x_1(\theta) \tag{4}$$

$$A(\theta) = 2\left(\frac{\pi D^2}{4}\right) + \pi D x_1(\theta) \tag{5}$$

$$x_1(\theta) = (l_c + R) - \left[R\cos\theta + \sqrt{\left(l_c{}^2 - R^2 \sin^2\theta\right)}\right] \tag{6}$$

The convective heat transfer coefficient is computed using the well-known Woschni correlation

$$h_{cg} = 3.26 D^{-0.2} P^{0.8} T^{-0.55} w^{0.8}, \tag{7}$$

where the velocity of the burned gas w is given by

$$w = c_1 S_p + c_2 \frac{V_d T_r}{p_r V_r}\left(P(\theta) - P_m\right). \tag{8}$$

Specific heats, enthalpies, and internal energy of individual species in the working fluid were computed by using polynomials as follows.

$$\frac{C_{p,k}}{R_u} = a_{1,k} + a_{2,k} T + a_{3,k} T^2 + a_{4,k} T^3 + a_{5,k} T^4 \tag{9}$$

$$C_{v,k} = C_{p,k} - R_u \tag{10}$$

$$H_k = \left(a_{1,k} + \frac{a_{2,k}}{2} T + \frac{a_{3,k}}{3} T^2 + \frac{a_{4,k}}{4} T^3 + \frac{a_{5,k}}{5} T^4 + \frac{a_{6,k}}{T}\right) R_u T \tag{11}$$

$$U_k = H_k - R_u T \tag{12}$$

Mixture-averaged values of specific heat of the working fluid were averaged by using mole fractions as follows.

$$\overline{C}_v = \sum_{k=1}^{K} X_k C_{v,k}; \quad \overline{C}_p = \sum_{k=1}^{K} X_k C_{p,k}$$
$$\gamma = \frac{\overline{C}_p}{\overline{C}_v} \tag{13}$$

A similar procedure was used to compute the mixture-averaged values of enthalpy and internal energy of the working fluid. As explained earlier, computing the value of γ based on the temperature and mixture composition of the working fluid is essential in order to obtain greater accuracy in the prediction of cylinder pressure and consequently the cylinder temperature, wall temperature, and emissions.

The Wiebe function was used to compute the burned mass fraction [34],

$$x_b(\theta) = \frac{m_{fb}}{m_{fT}} = \left\{1 - \exp\left\{-a\left(\frac{\theta - \theta_0}{\theta_b}\right)^{m+1}\right\}\right\} \tag{14}$$

where θ, θ_0, and θ_b are the instantaneous crank angle, the crank angle for the start of combustion, and the combustion duration, respectively. Further, m_{fb} is the fuel burned, m_{fT} is the total fuel at BDC, and $x_b(\theta) - x_b(\theta - 1)$ is the fraction of fuel burned in each crank angle and is used to compute Q_{in} in Eq. (2). The Wiebe function parameters, namely, a and m, shown in Eq. (14), are functions of various parameters (such as fuel type, equivalence ratio, load, speed etc). In this work, these user-defined parameters are fixed for all design/optimization conditions. However, the framework presented in this work allows the user to incorporate models describing a and m as functions of the above-mentioned engine parameters.

Based on the temporal variation of the cylinder pressure ($P(\theta)$), the average gas temperature was obtained as

$$T(\theta) = \frac{P(\theta) V(\theta)}{m(\theta) R_g}. \tag{15}$$

Figure 2 shows a schematic of the two-zone combustion model used in this work. The infinitesimally thin flame front separating the burned and unburned zone is shown in red.

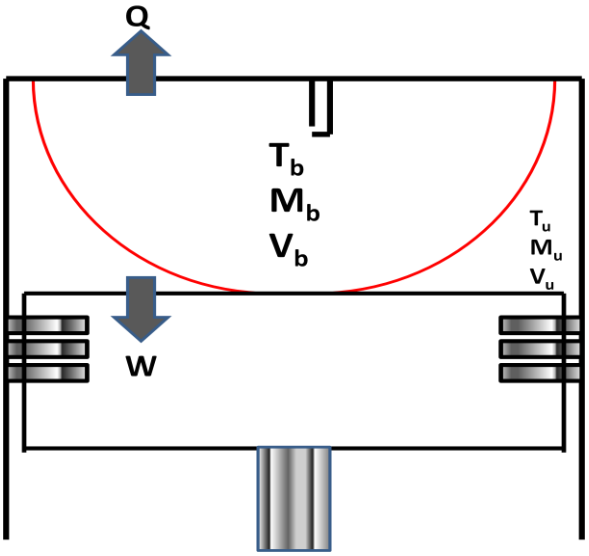

Figure 2: Schematic of the two zones (burned and unburned) in the engine chamber.

The burned and unburned gas temperatures were obtained as

$$T_b(\theta)=\frac{P(\theta)V_b(\theta)}{m_b(\theta)R_{gb}} \tag{16}$$

$$T_u(\theta)=\frac{P(\theta)V_u(\theta)}{m_u(\theta)R_{gu}}, \tag{17}$$

where the subscripts "u" and "b" represent unburned and burned quantities, respectively. The volume fraction of the burned gas y_b ($=V_b/V$) can be obtained by using the following relationship [34].

$$x_b(\theta)=\left[1+\frac{\rho_u}{\rho_b}\left(\frac{1}{y_b}-1\right)\right]^{-1} \tag{18}$$

Following [34], $\frac{\rho_u}{\rho_b}=4.0$ was used for the sake of simplicity. The effect of the assumed ratio, $\frac{\rho_u}{\rho_b}$, on the burned gas temperature was investigated in an earlier work [35]. The ratio of $\frac{\rho_u}{\rho_b}$ affects the burned gas temperatures for small values of burned gas fraction $x_b(\theta)$. From Eq. (18), one can see that as $x_b(\theta)$ tends to unity, the influence of the density ratio is insignificant. As discussed in [35], for $x_b(\theta) > 0.9$, the difference in burned gas temperature between $\frac{\rho_u}{\rho_b}=3.0$ and $\frac{\rho_u}{\rho_b}=5.0$ was less than 3%.

The moles of CO_2, H_2O, O_2, and N_2 produced in CAD $d\theta$ in accordance with the single-step global chemistry model are as follows.

$$n_{co2}(d\theta)=x_1\left(x_b(\theta)-x_b(\theta-d\theta)\right)/M_f \tag{19}$$

$$n_{H2O}(d\theta)=\frac{y_1}{2}\left(x_b(\theta)-x_b(\theta-d\theta)\right)/M_f \tag{20}$$

$$n_{o2}(d\theta)=\left(\frac{1}{\phi}-1\right)\left(x_1+\frac{y_1}{4}\right)\left(x_b(\theta)-x_b(\theta-d\theta)\right)/M_f \tag{21}$$

$$n_{N2}(d\theta)=\left(\frac{\beta}{\phi}\right)\left(x_1+\frac{y_1}{4}\right)\left(x_b(\theta)-x_b(\theta-d\theta)\right)/M_f \tag{22}$$

In Eqs. (19) through (22), x_1 and y_1 are the number of carbon and hydrogen atoms in the fuel respectively, β is the N_2:O_2 ratio in air, which is taken to be 3.76; and M_f is the molecular mass of the fuel.

The total number of moles of any specie (CO_2, H_2O, O_2, and N_2) in the burned zone at any crank angle θ is

$$n_N(\theta)=\sum_{\theta=\theta i}^{\theta=\theta}n_N(d\theta), \tag{23}$$

where the summation is over the crank angle interval from θ_i (SOI) to θ. Since the initial moles of fuel, O_2, and N_2 are known, the composition of the unburned zone can be computed based on Eqs. (19)–(23).

Emissions Model

The emissions model uses the instantaneous values of cylinder temperature (burned gas for the two-zone model, or average temperature for the single-zone model), pressure, and mixture composition to compute the engine-out NO and CO using reaction-rate-controlled models or reduced finite-rate chemistry models. The methodology to compute the temporal variation of NO using a reduced chemistry model is described in detail in [36]. The reaction rate-controlled models for NO and CO are described next.

Reaction-rate-controlled NO model

The extended Zeldovich mechanism is used to derive a rate expression for the time rate of change of NO concentration; for details, see [34]. Table 1 shows the reactions in the extended Zeldovich mechanism (units cm^3, gmol, s, K) where, K_i^+ and K_i^- represent the forward and backward reaction rates of the *i*th reaction (*i* = 1, 2, or 3), respectively. Based on the extended Zeldovich mechanism, the time rate of change of NO is

Table 1: Extended Zeldovich mechanism with rates [34].

	Reaction	$\mathbf{K_i}$+	$\mathbf{K_i}$-
1	$O + N_2 = NO + N$	$7.6\text{x}10^{13}$ $\exp(-3.8\text{x}10^4/T)$	$1.6\text{x}10^{13}$
2	$N + O_2 = NO + O$	$6.4\text{x}10^9$ T $\exp(-3150/T)$	$1.5\text{x}10^9$T $\exp(-1.95\text{x}10^4/T)$
3	$OH + N = NO + H$	$4.1\text{x}10^{13}$	$2.0\text{x}10^{14}$ $\exp(-2.365\text{x}10^4/T)$

$$\frac{d[NO]}{dt} = k_1^+[O][N_2] + k_2^+[N][O_2] + k_3^+[N][OH] - k_1^-[NO][N] - k_2^-[NO][O] - k_3^-[NO][H]. \quad (24)$$

Following the assumptions outlined in [34], Eq. (24) can be written as

$$\frac{d[NO]}{dt} = 2k_1^+[O][N_2] - 2k_1^-[NO][N]. \quad (25)$$

The concentration for [N] in Eq. (25) can be written as

$$[N] = \frac{k_1^+[O][N_2] + k_2^-[NO][O] + k_3^-[NO][H]}{k_3^+[OH] + k_1^-[NO] + k_2^+[O_2]}. \quad (26)$$

Equilibrium concentrations of O, N_2, NO, H, OH, and O_2 are used in computing the RHS of Eqs. (25) and (26). The rate-controlled model for NO described above is sometimes referred to as the Heywood model. The rate constants and equilibrium concentrations of species used in evaluating Eq. (25) are computed by using the burned gas temperature and pressure at a given crank angle. Effects of mixing between the burned and unburned gas and the temperature gradients in the burned gas region are neglected. Solution of Eq. (25) yields the temporal variation of NO concentration (in moles/cm^3).

Equation (25) describes the temporal change in the NO concentration when the volume is constant. Since the volume of the cylinder is constantly changing during the compression and power strokes of the IC engine, Eq. (25) needs to include the effect of changing cylinder volume on the NO concentrations. Reference [33] discusses an extension of Eq. (25) to include the effect of burned zone volume. Since $[NO] = \frac{N_{NO}}{V}$, where N_{NO} is the number of moles of NO, the LHS of Eq. (25) can be rewritten as

$$\frac{d[NO]}{dt} = \frac{d}{dt}\left[\frac{N_{NO}}{V}\right] = \frac{1}{V}\frac{dN_{NO}}{dt} + \frac{d}{dt}\left(\frac{1}{V}\right)N_{NO} \quad (27)$$

which can be shown to yield

$$\frac{d[NO]}{dt} = \left.\frac{d[NO]}{dt}\right|_H - [NO]\frac{1}{V_b}\frac{dV_b}{dt}, \quad (28)$$

where $\left.\frac{d[NO]}{dt}\right|_H$ is the rate of change of NO concentration at constant volume (Heywood model) computed by using Eq. (25). The second term on the RHS of Eq. (28) accounts for the decrease in NO concentration as a result of increasing cylinder volume during the expansion stroke.

From SOI to EOC, the burned volume V_b can be computed based on the procedure discussed earlier. After EOC, $V_b = V(\theta)$, where $V(\theta)$ is the cylinder volume at crank angle θ.

Reaction-rate-controlled CO model

The reaction rate-controlled CO model used in this work is an adaptation of the model discussed in [6]. Equation (28) in [6] does not include the effect of changing volume. Similar to Eq. (28) shown above, the CO model used in this work can be written as $\frac{d[CO]}{dt} = \left.\frac{d[CO]}{dt}\right|_{cv} - [CO]\frac{1}{V_b}\frac{dV_b}{dt}$, (29)

where $\left.\frac{d[CO]}{dt}\right|_{cv}$ is the rate of change of CO concentration at constant volume. The CO formation and the forward reaction rates are given in [6] and rewritten for the convenience of the reader. As in [6], the backward reaction rates are computed by using equilibrium considerations:

Table 2: CO formation mechanism with rates [6].

	Reaction	$\mathbf{K_f}$
1a	$CO + OH = CO_2 + H$	$1\text{x}10^{13}\exp(-8.05\text{x}10^3/T)$
1b	$CO + OH = CO_2 + H$	$1.01\text{x}10^{11}\exp(-30.0698/T)$
1c	$CO + OH = CO_2 + H$	$9.03\text{x}10^{11}\exp(-2.30\ \text{x}10^3/T)$
2	$CO_2 + O = CO + O_2$	$2.5\text{x}10^{12}\exp(-2.41\ \text{x}10^4/T)$
3	$CO + O + M = CO_2 + M$	$1.54\text{x}10^{15}\exp(-1.5\ \text{x}10^3/T)$

$$\left.\frac{d[CO]}{dt}\right|_{cv} = \left(C_{co}R_1 + R_2 + R_3\right)\left(1 - \frac{[CO]}{[CO]_{eq}}\right) \quad (30)$$

$$R_1 = \left(k_{f,1a} + k_{f,1b} + k_{f,1c}\right)[CO]_{eq}\,[OH]_{eq} \quad (31)$$

$$R_2 = \left(k_{b,2}\right)[CO]_{eq}\,[O_2]_{eq} \quad (32)$$

$$R_3 = \left(k_{f,3}\right)[CO]_{eq}\,[O]_{eq}[M]_{eq}, \quad (33)$$

where [M] is written as

$$[M] = [H_2] + 6.5\,[H_2O] + 0.4\,[O_2] + 0.4\,[N_2] + 0.75[CO] + 1.5[CO_2], \quad (34)$$

where all the values used in computing [M] in Eq. (34) are equilibrium values computed at the temperature and pressure at a particular crank angle.

Thermal Model

Assuming that the heat transfer occurs only in the direction perpendicular to the engine wall and that there is no heat loss from the top of the engine or the piston surface, one can develop a 1-D model to compute the transient temperature distribution in the engine wall using the heat conduction equation

$$\frac{dT_w(t)}{dt} = \frac{1}{\alpha}\frac{d^2T_w(t)}{dx^2}, \quad (35)$$

where α is the the thermal diffusivity. On the coolant side of the wall (x = 0), the temperature is held constant at T_c. On the engine side (x = L, where L is the engine wall thickness), the heat flux on the wall is balanced by heat conducted through the engine wall:

$$K\frac{dT_w(t)}{dx} = h_c(t)\left(T_g(t) - T_w(t)\right). \quad (36)$$

The heat transfer coefficient $h_c(t)$ and T_g are functions of time; they change during the course of the compression and expansion stroke. The simplified thermal model presented above can easily be extended to include the heat loss from the top of the cylinder as well as to the piston head. The heat transfer coefficient used in Eq. (36) is the same as Eq. (7), but can also be a user-input.

Optimization Model

We let $x \in R^n$ denote a generic vector of *n* design parameters (such as $x_1 = \theta_i$, $x_2 = \phi$, $x_3 = m_{fT}$, …). We typically constrain each of these parameters to lie within lower and upper bounds, so that $l_j \le x_j \le u_j$ for $j=1,\ldots,\ n$ (where $l_j < u_j$) denotes the feasible design region. These bounds correspond to physical limitations or design considerations. For instance, the limits of injection timing might be $-30° \le \theta_i \le -4°$, and the range of the equivalence ratio might be $0.65 \le \phi \le 1.0$ depending on operating conditions.

Using this notation, we can immediately formulate simple bound-constrained problems, such as maximizing torque:

$$max_x\ \boldsymbol{T}(x_1, x_2 \ldots, x_n)$$

$$\text{subject to } l_j \le x_j \le u_j \text{ for } j=1,\ldots,\ n, \quad (37)$$

where $\boldsymbol{T}(x)$ denotes the (brake) torque as a function of the design parameter values *x*.

In practice, one tends to also be interested in parametric studies. For example, given values $(x_2 \ldots x_n)$ for the remaining parameters, the ignition timing that achieves the maximum brake torque can be defined as

$$\theta_i^*(x_2, \ldots, x_n) = \arg\max_{x_1}\{\boldsymbol{T}(x_1, \ldots, x_n): (l_1 \le x_1 \le u_1)\}, \quad (38)$$

where we implicitly assume that there is a unique value of θ_i in the interval $[l_1,u_1]$, at which the torque is maximized.

Based on the maximum brake torque, one can formulate *bilevel* optimization problems based on the emissions, which we use in this paper to illustrate our approach. For example, one can envision minimizing the NO emissions along the maximum brake torque curve:

$$min_x\ N(x_1, x_2 \ldots, x_n)$$

$$\text{subject to } x_1 = \theta_i^*(x_2, \ldots, x_n) \quad (39)$$

$$l_j \le x_j \le u_j, \quad j=2,\ldots,n,$$

where $N(x)$ denotes the engine-out NO as a function of the design parameter values *x*. A problem with Eq. (39) is that it can often result in underperforming designs in terms of torque because it favors solutions to the top-level problem of minimizing NO. Furthermore the solutions tend to lie at the boundaries of the hyper-rectangle $[l_2,u_2]\ x \ldots x\ [l_n,u_n]$.

Instead, one often identifies the worst-case NO along the maximum brake torque curve.

$max_x\ N(x_1, x_2\ \ldots, x_n)$

$subject\ to\ x_1 = \theta_i^*(x_1, x_2, \ldots, x_n),$

$l_j \leq x_j \leq u_j, \quad j=2,\ldots, n$ (40)

For example, when n=2, x_1 denotes the ignition timing (θ_i), and x_2 denotes the equivalence ratio (ϕ), Eq. (40) corresponds to the case of obtaining the value of ϕ at which the NO is maximized for MBT.

Alternatively, our model also allows us to formulate problems where torque is maximized subject to constraints on the emissions (e.g., engine-out NO or CO). Details of the analogous optimization approach for such nonlinear simulation-constrained problems can be found in [31].

The chief limitation of traditional "black-box" approaches to solving Eq. (40) is that they require one focusing on the reduced problem.

$max_{x2,\ldots,xn} \quad N(\theta_i^*(x_2, \ldots, x_n), x_2, \ldots, x_n)$

$subject\ to\ l_j \leq x_j \leq u_j, \quad j=2,\ldots, n$ (41)

Consequently, for each value of the *(n-1)*-dimensional design vector $(x_2, \ldots, x_n)$, a 1-D nonlinear, simulation-based problem, Eq. (38), must be solved. Doing so adds considerable expense in terms of the numbers of simulation evaluations that must be performed. Furthermore, this reduced approach ignores the fact that for each of the simulation evaluations of torque done to obtain $\theta_i^*(x_2, \ldots, x_n)$, the additional cost of also obtaining NO at these design parameter values maybe negligible.

Therefore, in our approach, we solve only the lower-level problem Eq. (38) approximately for a given $(x_2, \ldots, x_n)$ and then determine the next value of $(x_2, \ldots, x_n)$ to evaluate based on both this approximate solution and the upper-level objective N. Formally, this means that for each of the, say, *d* design vector values

$$x^k = (x_1^k, x_2^k, \ldots, x_n^k), \qquad k = 1, \ldots, d$$

for which a simulation has been run, we employ the simulation outputs

$$\{N(x^k), \boldsymbol{T}(x^k)\}, \qquad k = 1, \ldots, d$$

to form quadratic surrogates q^N and q^T of N and **T**, respectively.

We can use these surrogates to solve a sequence of problems

$max_x\ q^N\ (x_1, x_2, \ldots, x_n)$

subject to $\frac{\partial q^T(x_1, x_2, \ldots x_n)}{\partial x_1} = 0,$

$l_j \leq x_j \leq u_j, \quad j=1, \ldots n,$

$(x_1, x_2, \ldots, x_n) \in \Omega\ ,$ (42)

where the surrogates are updated with each simulation evaluation. We restrict our attention to a local neighborhood Ω of the current design iterates.

Figure ***3*** (a) and (c) shows initial quadratic surrogates for NO and torque formed locally about the point (0.8,-20) based on the output of four simulations. When a fifth simulation is performed (at (0.9,-20)), the models are updated taking into account this new information as shown in Figures 3 (b) and (d). The domain Ω in which these models are trusted is similarly updated; for further details of this methodology we refer the reader to [30].

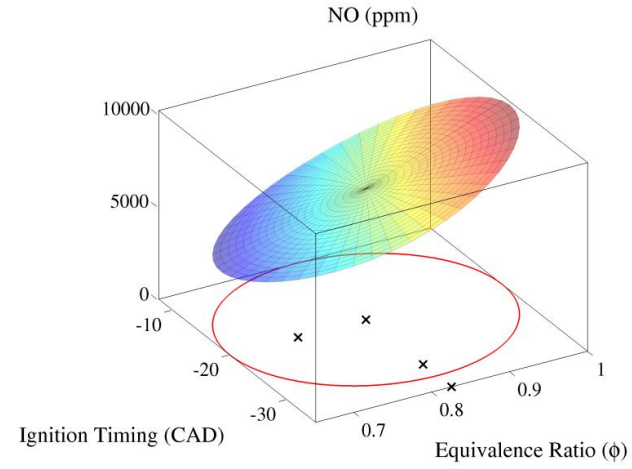

(a)

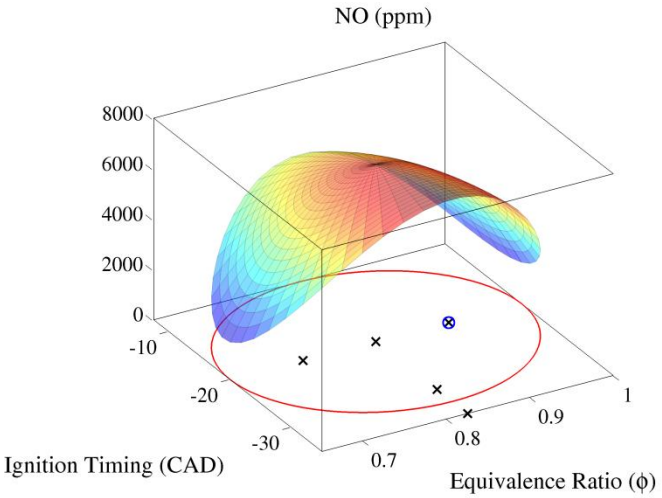

(b)

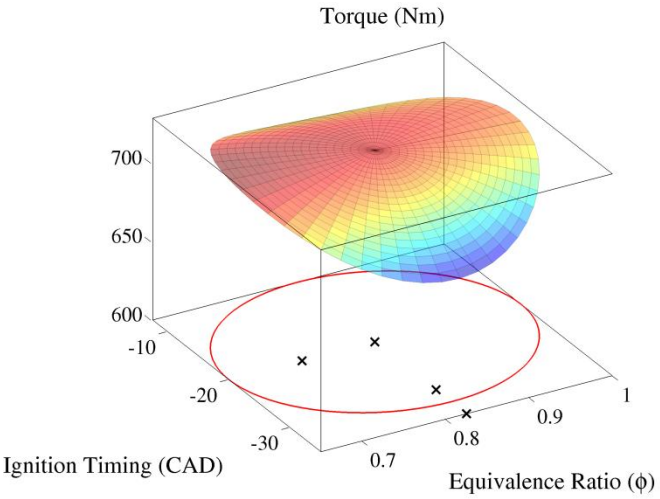

(c)

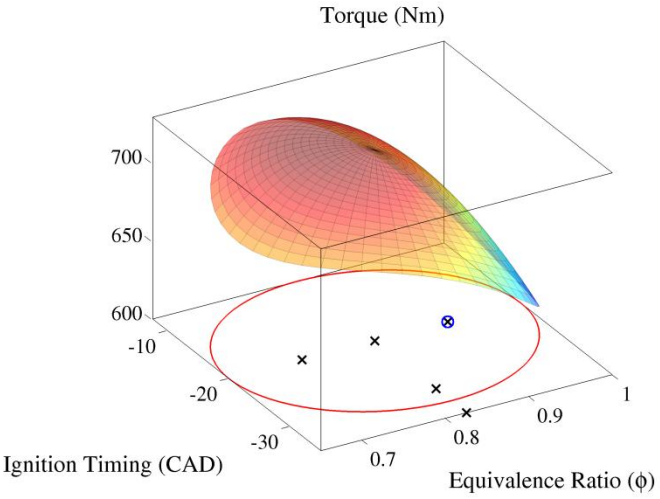

(d)

Figure 3: Example quadratic surrogate updates for NO (b) and torque (d) after a fifth value of x is evaluated. The boundary of the domain Ω in which the models are currently trusted is indicated by a red circle.

The main advantage of Eq. (42) is that it involves polynomial functions q^T and q^N that are algebraically available and hence trivial to optimize over, in contrast to the respective simulation-based functions **T** and N in Eq. (40). A secondary benefit from this implementation is that the constraint associated with the lower-level problem, Eq. (38), is only approximately solved at each iteration.

METHOD OF SOLUTION

The numerical procedure to obtain the cylinder pressure in a diesel engine is explained in detail in [32]. The same procedure was adapted to obtain the pressure and temperature in an SI engine by using the equations described above. Briefly, for a given set of operating conditions, namely, the prescribed mass of the fuel-air mixture and temperature at BDC, Eq. (1) was solved iteratively by using Eqs. (2)–(14) to obtain the pressure from $-179° < \theta < 180°$, in increments of 1°. For a given pressure at a crank angle, the burned and unburned gas temperatures were obtained by using Eqs. (16) and (17).

In order to compute the temporal variation of the wall temperature in Eq. (3), user-defined values of the cold start temperature ($T_w(0)$) and coolant temperature (T_c) are needed. Based on these values, Eqs. (35) and (36) were solved to obtain the wall temperature, $T_w(t)$. At each crank angle (or time based on the engine speed), the average engine gas temperature and Eq. (35) (subject to a boundary condition of the wall on the coolant side and engine cylinder side) are iterated to obtain the wall temperature. This procedure is used to compute the engine wall temperature for all crank angles.

Knowing the temperature, pressure, and elemental mixture composition, one can compute the temporal variation of emissions (NO and CO) described by Eqs. (28) and (29). The equilibrium concentrations required to compute Eqs. (28) and (29) are computed by using a well-validated, fast, robust method described in detail in [37].

RESULTS AND DISCUSSION

This section discusses the sample results from each of the models in the engine module. It also discusses performance maps showing the influence of ignition timing, equivalence ratio, fuel mass, and engine speed that are useful in making design and/or optimization decisions based on trade-offs, such as torque and emissions or fuel economy and torque. As an example, the tool was used to study a large-bore stationary natural gas engine described in [38]. The nominal value of fuel was 0.13 g/cycle as in [38], and the nominal engine RPM was 1800. Validation of the results of the engine and emissions module has been included in a companion paper (2013-24-0134) and hence not repeated here. Temporal variation of pressure and engine-out NO and CO over a range of equivalence ratios compared well with experimental data.

Figure 4 shows the average cylinder pressure for various ignition timings. Advancing ignition timing leads to a higher peak pressure, as expected.

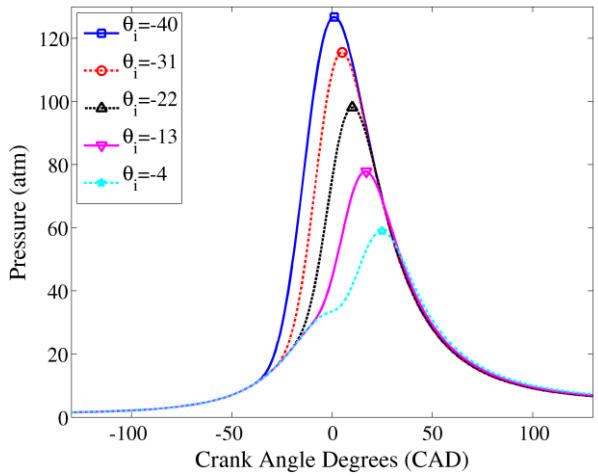

Figure 4: Variation of cylinder pressure with crank angle for various values of ignition timing (θ_i).

Figure 5 shows the variation of the average gas temperature for different values of ignition timing (computed by using Eq. (15)). The temporal variation of average temperature follows the pressure shown in Figure 4. Advancing the spark timing leads to higher peak temperatures corresponding to higher peak pressures. Furthermore, advancing spark timing also lowers the exhaust temperature for a given load (i.e., mass of fuel burned per cycle).

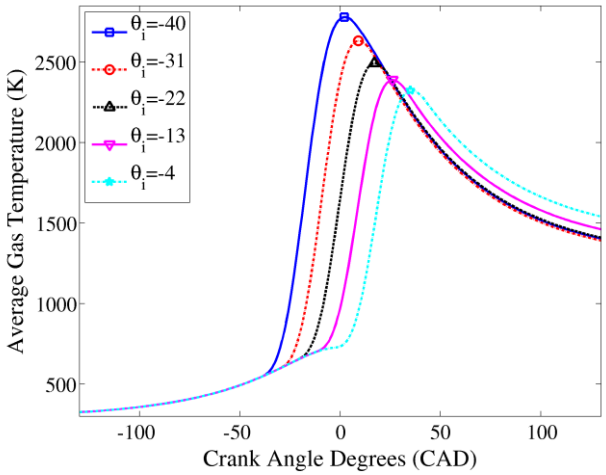

Figure 5: Temporal variation of average gas temperature for various values of ignition timing (θ_i).

Figure 6 shows the temporal variation of the engine-out NO as a function of ignition timing. Advancing the spark timing increases the engine out NO. This result is consistent with the production of higher engine peak temperature occurring on account of advancing spark timing.

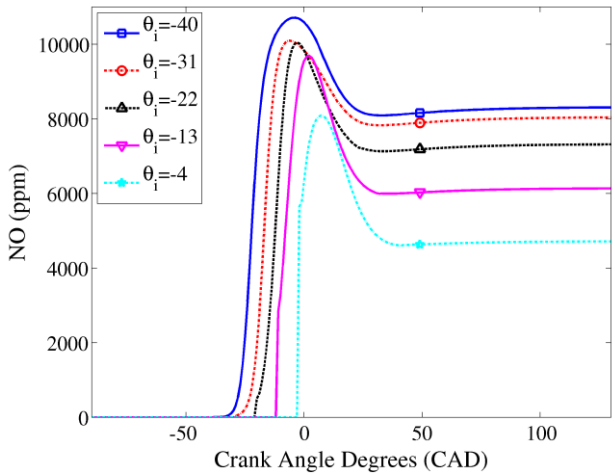

Figure 6: Temporal variation of NO (ppm) with crank angle for various values of ignition timing (θ_i).

Figure 7 shows the temporal variation of CO as a function of crank angle for various ignition timings. Retardation of the spark timing leads to higher engine-out CO emission. This result is consistent with the fact that higher peak engine temperatures lead to more complete combustion of the fuel into CO_2 as opposed to CO.

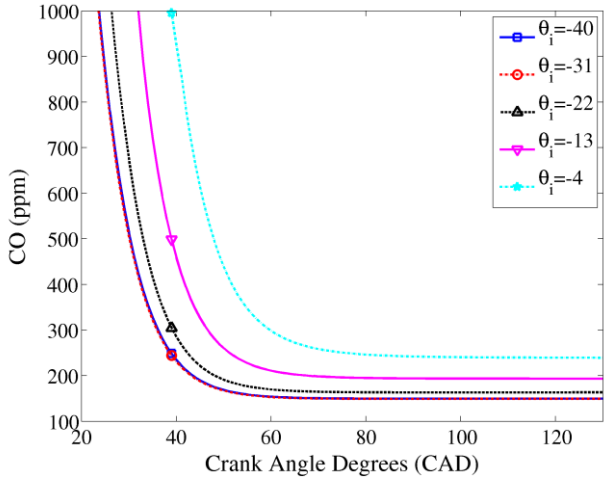

Figure 7: Temporal variation of CO (ppm) with crank angle for various values of ignition timing (θ_i)

Figures 4 to 7 show the results of the engine and emission models. Sample results from the thermal model are discussed next. Figures 8 and 9 show the temporal variation of the engine gas temperature and wall heat transfer coefficient. One can see that the engine wall is subject to highly transient heat fluxes on account of the sharp rise in gas temperature (and heat transfer coefficient, h_{cg} in Eq. (3)) when combustion and heat release occur close to TDC followed by longer periods of low heat flux. Figure 10 shows that this transient heat flux penetrates into a thin layer of the engine wall adjacent to the combusting gas, whereas the remaining portion of the wall is

"shielded" from these highly transient heat fluxes. These results are consistent with previously reported 1-D engine wall thermal models [39].

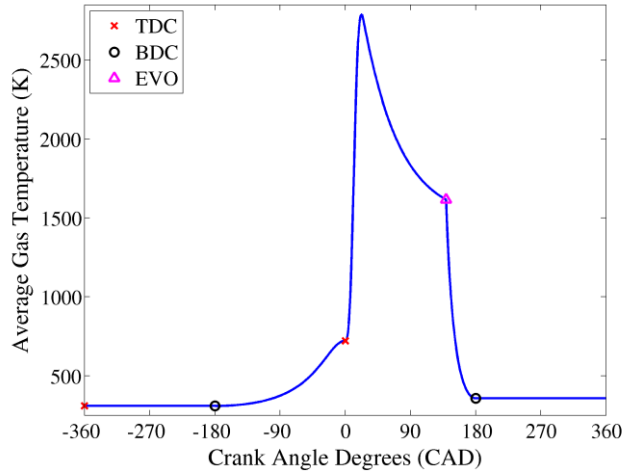

Figure 8: Variation of gas temperature as a function of crank angle (intake, compression, expansion, and exhaust).

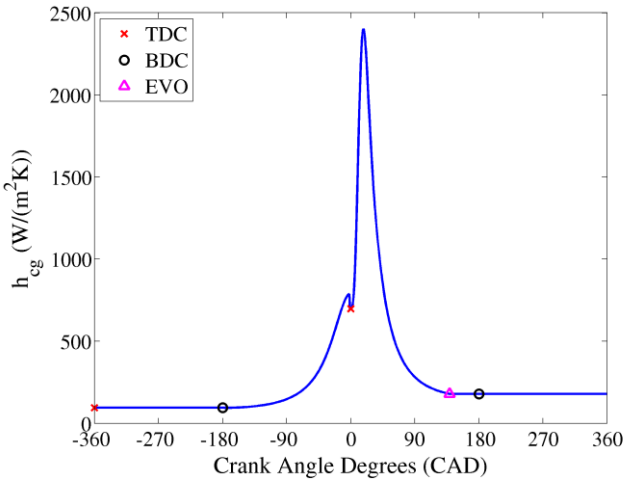

Figure 9: Variation of h_{cg} as a function of crank angle (intake, compression, expansion, and exhaust).

Figure 11 shows the temporal variation of the wall temperature in a transient engine cycle. The initial wall temperature was set at 300K, and the coolant temperature was fixed at 350K. The engine wall heats up in response to the gas temperature, and the average quasi steady-state temperature is about 400K.

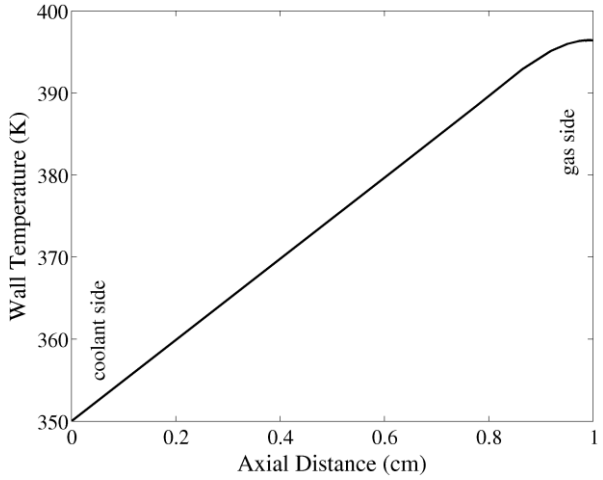

Figure 10: Axial variation of wall temperature.

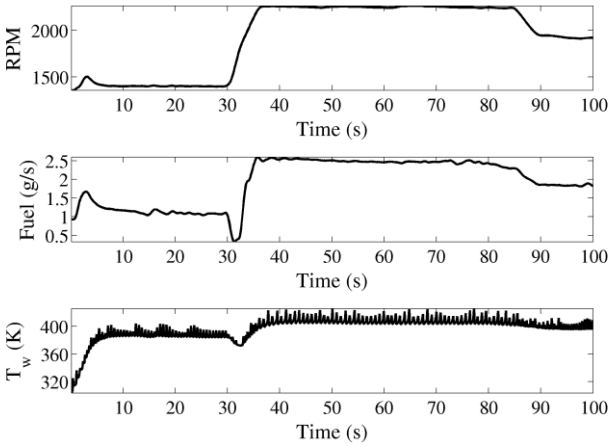

Figure 11: Temporal variation of T_w in a transient cycle.

As explained earlier, the engine module can be used for detailed parametric studies to study the impact of various operating parameters, such as fuel mass (proportional to load), engine speed, equivalence ratio, and ignition timing (θ_i). In these parametric studies, the equivalence ratio ϕ was varied from 0.65 to 1; and for each ϕ, the spark timing was varied from -40 to 0 CAD. Engine speed was varied from 1200 to 2400 RPM (in steps of 200 RPM for a total of 7 cases), and the fuel mass was varied from 90% to 110% (in steps of 2.5% for a total of 9 cases) of the nominal fuel mass, which was set equal to 0.13 gm/cycle. The nominal engine speed was 1800 RPM. For a given speed and load, 2500 cycle simulations were performed (50 each for ϕ and θ_i). Based on the range of parameters, a total of about 160,000 engine cycle simulations were conducted.

Figures 12 to 14 show contour plots of performance (torque) and emissions (NO and CO (ppm)) as a function of ignition timing and ϕ. The thick blue line shows the values corresponding to MBT (obtained from parametric studies by

varying θ_i for a given value of ϕ). For instance, Figure 12 shows that at $\phi = 0.7$, the spark timing corresponding to MBT is ≈ -26 and the MBT torque value is ≈730 N-m. As expected, the ignition timing has to be advanced at lower values of ϕ in order to obtain MBT torque values (at a given value of fuel and engine speed).

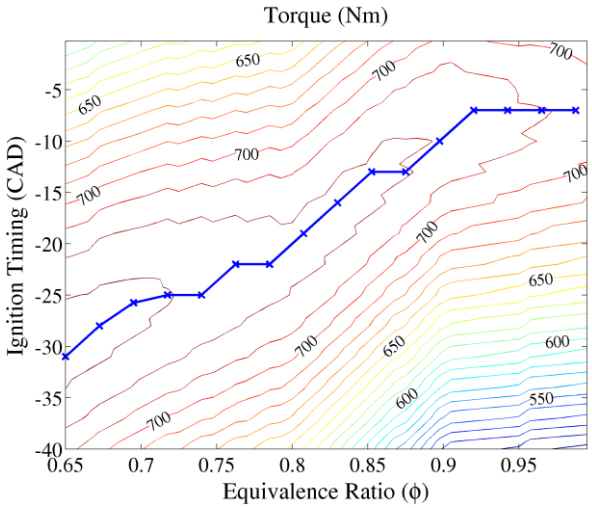

Figure 12: Contour plot of torque as a function of ignition timing (θ_i) and equivalence ratio (ϕ).

Figures 13 and 14 show contour plots of NO and CO (ppm), respectively, as functions of ignition timing and equivalence ratios, with the MBT curve superimposed on the emission plots. From these contour plots, one can obtain the NO and/or CO at MBT at a given ϕ and the corresponding θ_i. For instance, at $\phi = 0.75$, the NO corresponding to MBT is about 6750 ppm. Similar observations for CO can be drawn from Figure 14.

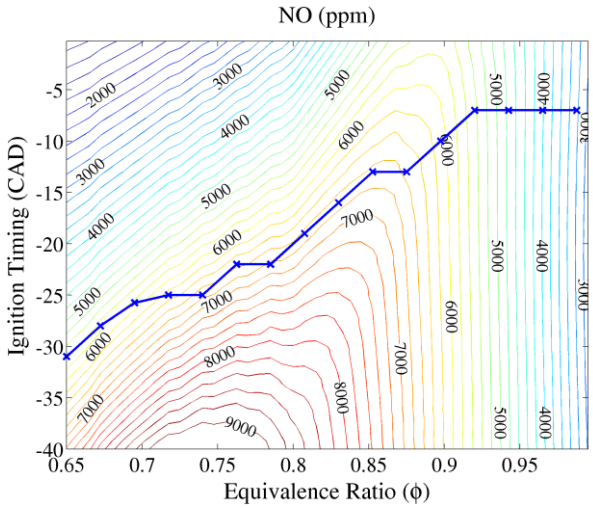

Figure 13: Contour plot of NO (ppm) as a function of ignition timing (θ_i) and equivalence ratio (ϕ).

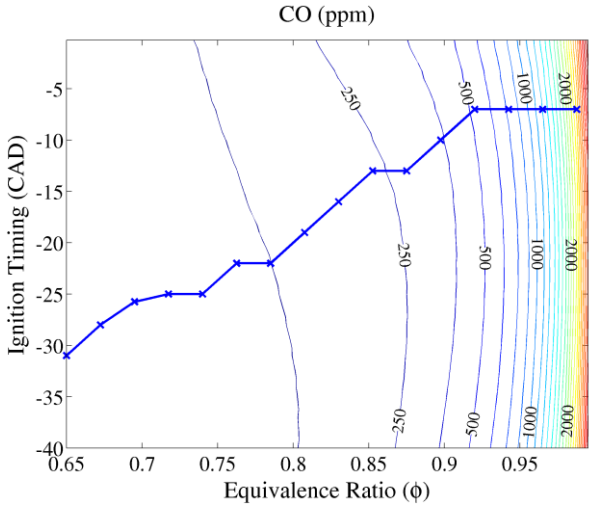

Figure 14: Contour plot of CO (ppm) as a function of ignition timing (θ_i) and equivalence ratio (ϕ).

Figures 15 to 18 show the engine-out NO and CO at MBT for a range of speeds and fuel masses (expressed as a percentage of the nominal value of 0.13 g/cycle). Figure 15 shows that the maximum NO at MBT occurs around $\phi = 0.8$ consistent with experimental data shown in Ref. [38]. Figures 15 and 16 also show that engine speed and load does not significantly impact either the value of ϕ_{max} (the value of ϕ that maximizes engine-out NO) or the magnitude of the maximum NO emission.

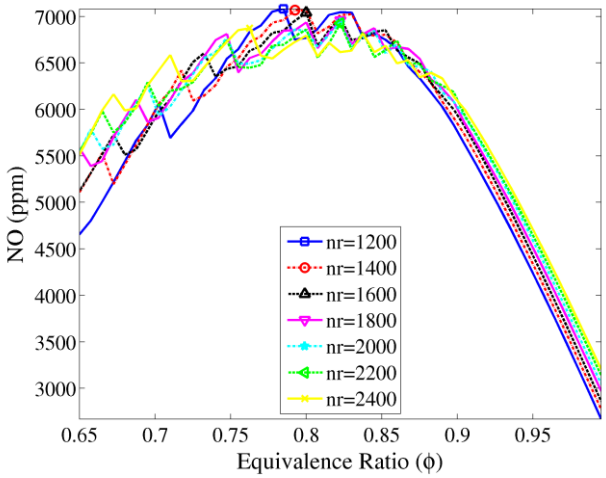

Figure 15: Impact of speed (RPM) on engine-out NO.

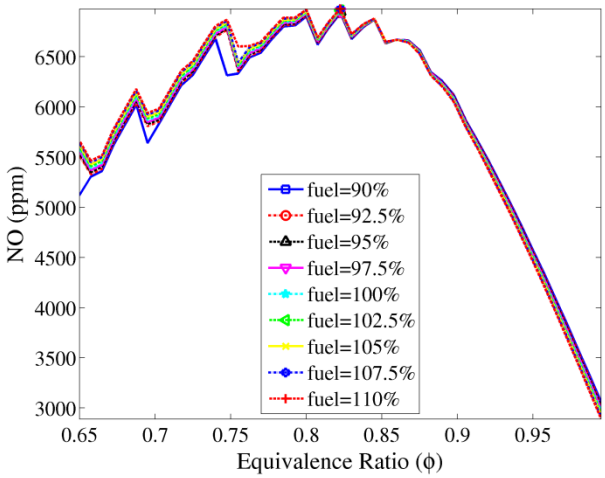

Figure 16: Impact of load (fuel mass as a % of nominal value) on engine-out NO.

Figure 17 shows that the engine speed impacts the engine-out CO fairly significantly at higher equivalence ratios. For instance, the engine-out CO at ϕ=0.95 and 1200 RPM is about 600 ppm, whereas it is over 1100 ppm at 2400 RPM.

Figure 18 shows the impact of the load on engine-out CO. At lower loads (90% nominal value), the engine-out CO is higher than at higher loads (110% nominal value).

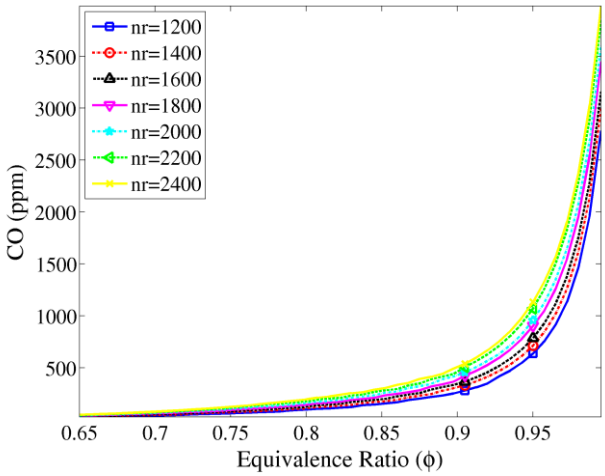

Figure 17: Impact of speed (RPM) on engine-out CO.

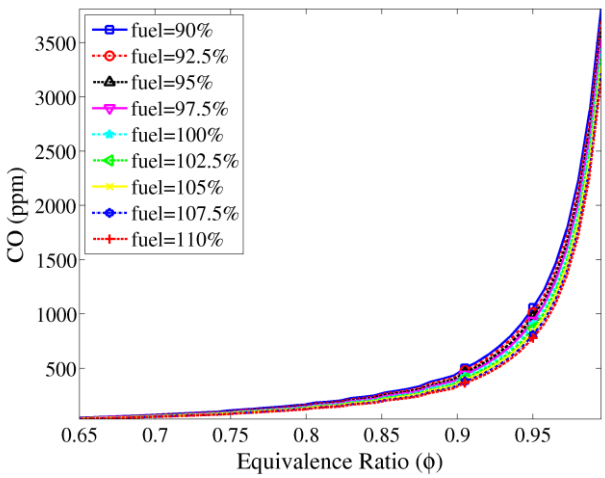

Figure 18: Impact of load (fuel mass as a % of nominal value) on engine-out CO.

Figure 19 shows the MBT curve superimposed on the contours of NO, which we would like to maximize as a function of ϕ and θ_i subject to being on the MBT curve (see Eq. (40)). On top of this we show the design points visited by two different optimization algorithms. The first (FMINCON) is obtained by using MATLAB's primary local optimization routine "fmincon" (which uses finite-difference estimates of the objective's derivatives) on the reduced problem (41) and requires 316 simulation evaluations. The second (POUNDER) is based on our previously described optimization module that directly exploits the bilevel structure in (40) and requires only 41 simulation evaluations. These design points were chosen iteratively by the each of the respective algorithms. The points chosen by FMINCON show that several ignition timing values need to be evaluated for each equivalence ratio value in order to solve the reduced problem. POUNDER more quickly focuses on the actual (top-level) problem of interest and therefore does not require as many total evaluations. Both routines find a maximum NO value on the MBT curve of approximately 6900 N-m, which is at least as good as the value obtained with a full parameter-space sweep requiring over 2500 simulation evaluations.

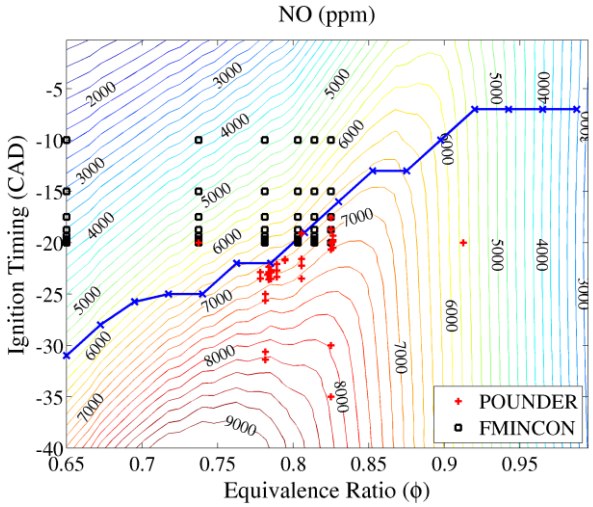

Figure 19: Comparison of the POUNDER scheme to compute ϕ corresponding to maximum NO at MBT compared with FMINCON.

SUMMARY/CONCLUSIONS

This paper discussed the development of an integrated tool for the design, optimization, and real-time control of engines from a performance and emissions standpoint. The tool was used to conduct parametric studies of the impact of various operating parameters such as load, engine-speed, equivalence ratio, and ignition timing on the engine performance (torque) and emissions (NO and CO).

Computational speed was a key consideration in the development of this design/optimization tool. A single engine cycle computation (which includes both performance and emissions) was performed in about 8 milliseconds on a single 2.53 GHz Intel processor. Efforts to study performance of the various modules on programmable ECUs (Engine Control Unit) are currently underway. Obtaining contour plots of performance and emissions for various operating conditions requires a large number of engine cycle simulations; hence computational speed is of prime importance. For example, in this work, 2500 evaluations were needed in order to obtain the MBT curve for a given load and speed. It was also shown that the optimization solver (an extension of the model-based derivative-free POUNDER) greatly reduces the number of engine model evaluations. In the particular optimization problem studied in this work, our optimization module reduced the number of evaluations by about two orders of magnitude as compared with parametric sweeps and about an order of magnitude compared with MATLAB's FMINCON. The computational speed of the engine module and the reduced number of evaluations as a result of the optimization scheme demonstrate the potential of this tool for real-time control and optimization.

It is clearly valuable for engine/emission modules to provide an optimization solver access to all the relevant quantities of interest (e.g., torque, CO, NO) because doing so allows a solver to reduce the number of required simulation evaluations. Pure "black-box" approaches aggregate all the output into a single merit/cost function and hence make optimization more computationally expensive. We expect that the advantage of structure-exploiting optimization routines that fully utilize the outputs of engine simulations will become even more pronounced as the number of design parameters, constraint functions, and/or objective functions increases. For example, a common problem involving a single additional design parameter (fuel) would be to minimize fuel consumption subject to sufficient torque and limits on NO and CO emissions. Alternatively, one could consider multi-objective problems where CO, NO, and fuel would be simultaneously minimized subject to constraints on the torque achieved. In these examples, the fuel design parameter occurs linearly as an objective (fuel consumption), and exploiting this knowledge is critical to reducing the simulation evaluations to a computationally feasible number.

REFERENCES

1. Dai, W., Davis, G., Hall, M., and Matthews, R., "Diluents and Lean Mixture Combustion Modeling for SI Engines with a Quasi-Dimensional Model," SAE Technical Paper 952382, 1995.
2. Jung, D., and Assanis, D., "Multi-Zone DI Diesel Spray Combustion Model for Cycle Simulation Studies of Engine Performance and Emissions," SAE Technical Paper 2001-01-1246, 2001.
3. Andersson, M., Johansson, B., Hultqvist, A., and Nöhre, C., "A Real Time NOx Model for Conventional and Partially Premixed Diesel Combustion," SAE Technical Paper 2006-01-0195, 2006.
4. Abu-Nada, E., Al-Hinti, I., Akash, B., and Al-Sarkhi, A., "Thermodynamic analysis of spark-ignition engine using a gas mixture model for the working fluid," International Journal of Energy Research 31, no. 11 (2007): 1031-1046.
5. Jung, D., and Assanis, D. N., "Quasi-dimensional modeling of direct injection diesel engine nitric oxide, soot, and unburned hydrocarbon emissions," Journal of Engineering for Gas Turbines and Power 128, no. 2 (2006): 388-396.
6. Perini, F., Paltrinieri, F., and Mattarelli, M., "A quasi-dimensional combustion model for performance and emissions of SI engines running on hydrogen–methane blends." International Journal of Hydrogen Energy 35, no. 10 (2010): 4687-4701.
7. Grill, M., Bargende, M., Rether, D., and Schmid, A., "Quasi-dimensional and Empirical Modeling of Compression-Ignition Engine Combustion and Emissions," SAE Technical Paper 2010-01-0151, 2010.
8. Grill, M., and Bargende, M., "The development of an highly modular designed zero-dimensional engine process calculation code," SAE Int. J. Engines 3(1):1-11, 2010.

9. Karra, P., and Kong, S., "Application of Particle Swarm Optimization for Diesel Engine Performance Optimization," SAE Technical Paper 2010-01-1258, 2010.
10. Shutty, J., "Control Strategy Optimization for Hybrid EGR Engines," SAE Technical Paper 2009-01-1451, 2009.
11. Ferrara, G., Ferrari, L., Vichi, G., and Varrocchi, A., "A Methodology for Engine Performance Optimization," SAE Technical Paper 2011-24-0156, 2011.
12. Fateh, N., Parashar, S., and Silvestri, J., "Game Theory Approach to Engine Performance Optimization," SAE Technical Paper 2008-01-0871, 2008
13. Millo, F., Perazzo, A., and Pautasso, E., "Optimizing the calibration of a turbocharged GDI engine through numerical simulation and direct optimization," SAE Int. J. Engines 3(1):556-570, 2010
14. Atkinson, C., Allain, M., Kalish, Y., and Zhang, H., "Model-Based Control of Diesel Engines for Fuel Efficiency Optimization," SAE Technical Paper 2009-01-0727, 2009.
15. Dumele, H., and Stangl, T., "Automated Map Optimization of a Large-Bore Diesel Engine," SAE Technical Paper 2011-01-0705, 2011.
16. Ge, H., Shi, Y., Reitz, R., Wickman, D., et al., "Engine Development Using Multi-Dimensional CFD and Computer Optimization," SAE Technical Paper 2010-01-0360, 2010.
17. Watson, H., Ratnawera, A., and Halgamuge, S., "Optimization of All SI Engine Combustion Control and Related Events for Efficiency," SAE Technical Paper 2006-01-0045, 2006.
18. D'Errico, G., and Cerri, T., "Application of Derivative-Free Search Algorithms for Performance Optimization of Spark Ignition Engines," SAE Technical Paper 2008-01-0354, 2008.
19. Mehrani, P., and Watson, H., "Joint Efficiency and NOx Optimization Using a PSO Algorithm," SAE Technical Paper 2006-01-1109, 2006.
20. Kuleshov, A., "Use of Multi-Zone DI Diesel Spray Combustion Model for Simulation and Optimization of Performance and Emissions of Engines with Multiple Injection," SAE Technical Paper 2006-01-1385, 2006.
21. Menegazzi, P., Albrecht, A., Millet, C., Aubret, P. et al., "A Simulation Tool for Vehicle Emissions, Consumption and Performance Analysis - Applications to DPF Modeling and DID Turbocharged Engine Control Design," SAE Technical Paper 2006-01-3004, 2006.
22. Watson, H., Ratnawera, A., and Halgamuge, S., "Optimization of All SI Engine Combustion Control and Related Events for Efficiency," SAE Technical Paper 2006-01-0045, 2006.
23. Geller, B., and Bradley, T., "Objective Comparison of Hybrid Vehicles through Simulation Optimization," SAE Technical Paper 2011-01-0943, 2011.
24. Gao, W., and Mi, C. "Hybrid vehicle design using global optimization algorithms," Int. J. Electric and Hybrid Vehicles 1, no. 1 (2007): 57-70, 2007.
25. Conn, A. R., Scheinberg, K., and Vicente, L.N., "Introduction to Derivative-Free Optimization." SIAM, Philadelphia, PA, 2009.
26. Tate, E., and Boyd, S., "Finding Ultimate Limits of Performance for Hybrid Electric Vehicles," SAE Technical Paper 2000-01-3099, 2000.
27. Griewank, A., and Walther, A., "Evaluating Derivatives: Principles and Techniques of Algorithmic Differentiation." SIAM, Philadelphia, PA, 2008.
28. Moré, J., and Wild. S.M., "Estimating derivatives of noisy simulations," ACM Transactions on Mathematical Software 38, no. 3 (2012): 1-19.
29. Wild, S. M.,"MNH: A Derivative-Free Optimization Algorithm Using Minimal Norm Hessians," Tenth Copper Mountain Conference on Iterative Methods, April 2008.
30. Munson, T., Sarich, J., Wild, S. M., Benson, S., and Curfman-McInnes, L. "TAO 2.0 Users Manual." Argonne National Laboratory Technical Memorandum ANL/MCS-TM-322, 2012.
31. Kannan, A., and Wild, S.M., "Benefits of Deeper Analysis in Simulation-based Groundwater Optimization Problems," Proceedings of the XIX International Conference on Computational Methods in Water Resources (CMWR 2012), June 2012.
32. Aithal, S. M., "Impact of EGR fraction on diesel engine performance considering heat loss and temperature-dependent properties of the working fluid," Int. J. Energy Research. 2008, 33**,** 415-430.
33. Andersson, I., and Eriksson, L., "A parametric model for ionization current in a four stroke SI engine," J. Dynamic Systems, Measurement and Control, 2009, 131 (2)s. 1-11.
34. Heywood, J. B., Internal Combustion Engine Fundamentals, McGraw-Hill, New York, 1988.
35. Aithal, S. M., "Analysis of the Current Signature in a Constant-Volume Combustion Chamber", Combust. Sci. Technol., 2013, 185(2), 336–349
36. Aithal, S. M. "Modeling of NO_x formation in diesel engines using finite-rate chemical kinetics," Applied Energy, 2010, 87(7), 2256-2265.
37. Aithal, S. M., "Development of a Fast, Robust Equilibrium Chemistry Solver for Analyses of Combustion Products", http://www.mcs.anl.gov/uploads/cels/papers/P1825-0111.pdf.
38. Biruduganti, M., Gupta, S., Bihari, B., McConnell, S., and Sekar, R., "Air separation membranes – an alternative to EGR in large bore natural gas engines," ASME Internal Combustion Engine 2009, Spring technical conference paper ICES2009-76054, 2009.
39. Morel, T., Keribar, R., and Blumberg, P., "Cyclical Thermal Phenomena in Engine Combustion Chamber Surfaces," SAE Technical Paper 850360, 1985

ACKNOWLEDGMENTS

This publication was created (or partially created) by UChicago Argonne, LLC as manager of Argonne National Laboratory for the U. S. Department of Energy under Contract No. DE-AC02-06CH11357.

DEFINITIONS/ABBREVIATIONS

A	surface area of cylinder head (m^2)
$a_{n,k}$	coefficients fits to thermodynamic data of k^{th} species
$C_{p,k}$	molar heat capacity at constant pressure of the k^{th} species (J/mole-K)
$C_{v,k}$	molar heat capacity at constant volume of the k^{th} species (J/mole-K)
$\overline{C}_p$	mixture-averaged molar specific heat at constant pressure (J/mole-K)
$\overline{C}_v$	mixture-averaged molar specific heat at constant volume (J/mole-K)
h_{cg}	convective heat transfer coefficient W m^{-2} K
H_k	molar enthalpy of the k^{th} species (J/mole)
H_P	enthalpy of the products (J)
H_R	enthalpy of the reactants (J)
l	vector of lower bounds for the design parameters
l_c	length of connecting rod
m	instantaneous mass in the engine cylinder (kg)
m_{fb}	mass of fuel (kg)
n	number of design parameters to be optimized over
N	engine-out NO as a function of input parameters x
N_{rpm}	rotational speed of the engine (rev/min)
$P(\theta)$	average cylinder pressure at crank angle θ (N/m^2)
Q_{in}	heat input from fuel combustion (J)
Q_{loss}	heat lost from engine cylinder (J)
R	crank radius (m)
R_g	gas constant (J/kg-K)
R_u	universal gas constant (J/K)
$T(\theta)$	average cylinder temp at crank angle θ (K)
T_w	wall temperature (K)
T(x)	torque as a function of input parameters x
u	vector of upper bounds for the design parameters
U_k	molar internal energy of the k^{th} species (J/mole)
$V(\theta)$	instantaneous volume at crank angle θ
$x_1(\theta)$	distance of cylinder head from TDC at θ
X_k	mole fraction of the k^{th} species

Greek Symbols

γ	ratio of specific heats
θ	crank angle
θ_i	ignition timing (CAD)
$\theta_i^*(x)$	the ignition timing as a function of x that maximizes torque
ϕ	equivalence ratio
ω	engine speed (= $6N_{rpm}$ deg/sec)

Abbreviations

ATDC	after top dead center
BDC	bottom dead center
CAD	crank angle degrees
EOC	end of combustion
EVO	exhaust value open
LHS	left-hand side
LHV	lower heating value
MBT	maximum brake torque
RHS	right-hand side
SI	spark ignition

SOI	start of ignition
TDC	top dead center